AD-A125 735 PARTICLE SIZE DETERMINATION IN SMALL SOLID PROPELLANT ROCKET MOTORS USING..(U) NAVAL POSTGRADUATE SCHOOL MONTEREY CA R G CRAMER OCT 82 1/1

UNCLASSIFIED F/G 21/8.2 NL

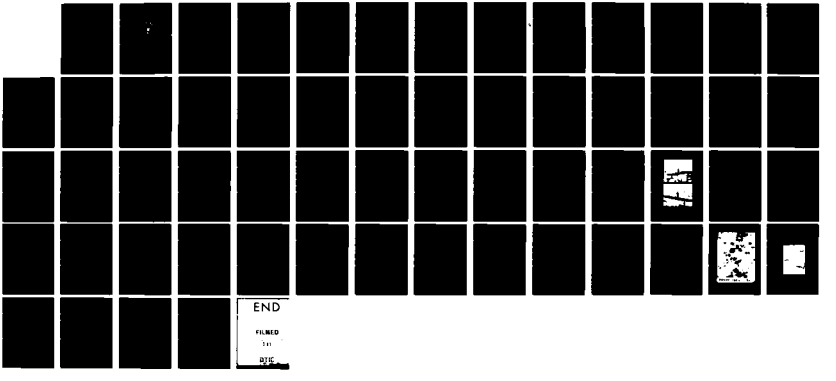

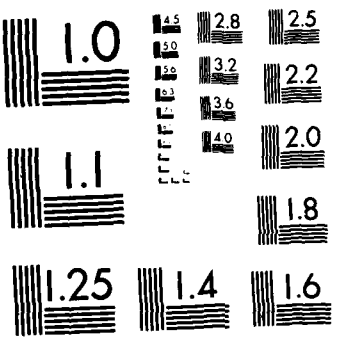

NAVAL POSTGRADUATE SCHOOL
Monterey, California

THESIS

PARTICLE SIZE DETERMINATION IN SMALL SOLID PROPELLANT ROCKET MOTORS USING THE DIFFRACTIVELY SCATTERED LIGHT METHOD

by

Robert Grewelle Cramer, Jr.

October 1982

Advisor: D. W. Netzer

Approved for public release; distribution unlimited

UNCLASSIFIED

SECURITY CLASSIFICATION OF THIS PAGE (When Data Entered)

REPORT DOCUMENTATION PAGE		READ INSTRUCTIONS BEFORE COMPLETING FORM
1. REPORT NUMBER	2. GOVT ACCESSION NO. AD-A125 735	3. RECIPIENT'S CATALOG NUMBER
4. TITLE (and Subtitle) Particle Size Determination in Small Solid Propellant Rocket Motors Using the Diffractively Scattered Light Method		5. TYPE OF REPORT & PERIOD COVERED Engineer's Thesis October 1982
		6. PERFORMING ORG. REPORT NUMBER
7. AUTHOR(s) Robert Grewelle Cramer, Jr.		8. CONTRACT OR GRANT NUMBER(s) F04611-82-X-0008
9. PERFORMING ORGANIZATION NAME AND ADDRESS Naval Postgraduate School Monterey, California 93940		10. PROGRAM ELEMENT, PROJECT, TASK AREA & WORK UNIT NUMBERS
11. CONTROLLING OFFICE NAME AND ADDRESS Air Force Rocket Propulsion Laboratory Edwards AFB, California 93523		12. REPORT DATE October 1982
		13. NUMBER OF PAGES 57
14. MONITORING AGENCY NAME & ADDRESS(if different from Controlling Office)		15. SECURITY CLASS. (of this report) Unclassified
		15a. DECLASSIFICATION/DOWNGRADING SCHEDULE

16. DISTRIBUTION STATEMENT (of this Report)

Approved for public release; distribution unlimited

17. DISTRIBUTION STATEMENT (of the abstract entered in Block 20, if different from Report)

18. SUPPLEMENTARY NOTES

19. KEY WORDS (Continue on reverse side if necessary and identify by block number)

Solid Propellant Rocket Motors

Metallized Propellants

Light Scattering

20. ABSTRACT (Continue on reverse side if necessary and identify by block number)

A dual beam apparatus was developed which simultaneously measured particle size (D_{32}) at the entrance and exit of an exhaust nozzle of a small solid propellant rocket motor. The diameters were determined using measurements of diffractively scattered laser power spectra. The apparatus was calibrated by using spherical glass beads and aluminum oxide powder. Measurements were successfully made at both locations. Because

DD FORM 1 JAN 73 1473 EDITION OF 1 NOV 68 IS OBSOLETE S/N 0102-014-6601

UNCLASSIFIED

SECURITY CLASSIFICATION OF THIS PAGE (When Data Entered)

of the presence of char agglomerates in the exhaust, continued effort is required to improve the grain design in order to obtain consistent "across nozzle" data.

Approved for public release; distribution unlimited

Particle Size Determination in Small Solid Propellant Rocket Motors Using the Diffractively Scattered Light Method

by

Robert Grewelle Cramer, Jr.
Captain, United States Army
B.S., Washington State University, 1973

Submitted in partial fulfillment of the requirements for the degrees of

MASTER OF SCIENCE IN AERONAUTICAL ENGINEERING

and

AERONAUTICAL ENGINEER

from the

NAVAL POSTGRADUATE SCHOOL
October 1982

Author: Robert G. Cramer Jr.

Approved by: Donald W. Platzer
Thesis Advisor

Harvey W. Bowden
Second Reader

Max F. Platzer
Chairman, Department of Aeronautics

William M. Tolles
Dean of Science and Engineering

ABSTRACT

A dual beam apparatus was developed which simultaneously measured particle size (D_{32}) at the entrance and exit of an exhaust nozzle of a small solid propellant rocket motor. The diameters were determined using measurements of diffractively scattered laser power spectra. The apparatus was calibrated by using spherical glass beads and aluminum oxide powder. Measurements were successfully made at both locations. Because of the presence of char agglomerates in the exhaust, continued effort is required to improve the grain design in order to obtain consistent "across nozzle" data.

TABLE OF CONTENTS

LIST OF TABLES

LIST OF FIGURES

ACKNOWLEDGMENT

In addition to my appreciation for the patience and understanding shown by my wife and sons, I would like to acknowledge the advice and assistance provided by Professor D. W. Netzer. Appreciation is also expressed to the members of the technical staff of the Aeronautical Engineering department, Messrs. R. Besel, P. Hickey, D. Harvey and R. Garcia, and especially to Mr. G. Middleton and Mr. T. Dunton, for their assistance and advice throughout this project. And finally, but not least, I would like to thank LT. B. J. Hansen, who supported me not only with his data acquisition system but with his friendship and encouragement, too.

I. INTRODUCTION

Aluminum is used as a fuel additive in solid propellants to increase the specific impulse of the rocket and to suppress high frequency combustion instability. Although there is an increase in specific impulse, the specific impulse efficiency may actually decrease when compared with the efficiency of the same base propellant without aluminum [Ref. 1]. This performance loss has been largely attributed to incomplete combustion of the aluminum and/or the formation of aluminum oxide particles in the motor cavity which leads to two-phase flow losses (i.e. velocity and thermal lags between the particles and the gas). The magnitude of the losses associated with these mechanisms has been reported to be 1% I_{sp} loss for 10% unburned aluminum and 2-10% loss in I_{sp} for two-phase flow effects [Ref. 2]. These losses are predicted analytically and at present there exists no adequate theoretical model relating particle size to propellant and motor parameters. Therefore, the accuracy of performance prediction is very dependent upon the accuracy of particle size data obtained experimentally.

The process by which aluminized fuel additives proceed to final combustion products is exceedingly complex. The final particle size is a function of several factors: original particle size, propellant properties, operating

environment (pressure, etc.) and the nozzle design and throat size [Ref. 2].

Kincaid and Derr [Ref. 3] have presented a comprehensive description of the process. A summary of their explanation is presented here. They divide the rocket motor into five zones: (1) at or near the propellant surface (0.5 to 5 mm); (2) within the motor cavity; (3) within the converging section of the nozzle; (4) at the nozzle throat; (5) within the diverging section of the nozzle. In zone (1), each particle is heated as it emerges at the surface. Its metal core melts, expands and eventually ruptures its surrounding oxide layer. Some of the original metal particles may ignite and leave the burning surface immediately. Other particles may accumulate on the surface in groups of 100 to greater than 1000--sometimes a million [Ref. 4]. These groups leave the surface either as clumps or burning droplets, called agglomerates. The aluminum oxide particles produced by aluminum combustion process have a bimodal size distribution. Fine material (1 μm) results from vapor phase combustion. This size is generally considered to be invariant and upon completion of aluminum combustion amounts to approximately 80% by weight of the total condensed phase products. Coarse material (100 μm) arises from breakup of the residual cap of Al_2O_3 on each burning particle. This large cap remains after the combustion of the metal has completed. The size of these particles is dependent on: propellant composition, pressure,

flow environment and the original size of the particle or agglomerate. It is believed that the degree of agglomeration on the surface will increase for highly aluminized propellants. Hence the proportion of coarse particles would increase.

Some oxidation occurs in zone (2), but the precise mechanism of oxidation is not known. In addition, some growth of Al_2O_3 particles by condensation and coagulation occurs in this zone. Behavior within zone (2) has been inferred from laboratory data. It has been suggested that the behavior in zone (2) would be dependent mainly on the size of the particles entering the zone. With increased agglomeration in zone (1) and short residence time in zone (2) the particles could enter the nozzle and be ejected prior to complete combustion. Another complication could be settling of the larger particles.

In zones (3), (4) and (5), size is affected by wall collisions, growth of particles, breakup of particles, condensation and solidification. Zone (3) is a region of accelerating gas velocity. When the two-phase flow of zone (2) enters this zone, collisions occur which lead to the growth of larger particles. As these particles accelerate, their break-up is also expected. Because of the change in cross-sectional area, the flow must turn and wall collisions occur. As the particles enter the throat of the nozzle (zone 4), particle breakup has been observed [Ref. 5]. As the flow expands through zone (5), it is cooled, and condensation and

solidification of the alumina occurs. The problem of two-phase flow losses occurs within zones (3)-(5) when the condensed phase material cannot maintain both velocity and thermal equilibrium with the gaseous phase. According to theory, condensed material smaller than 1 μm in diameter entering the nozzle will produce minimal two phase flow losses even for highly aluminized solid propellants.

At this time the Air Force Improved Solid Performance Program (SPP) uses a particle size model developed by Hermsen [Ref. 6], based on D_{43}, a weight (or DeBroucker) mean diameter. This model is based on correlation of a large amount of empirical data from many sources, most of which employed particle analysis of collected exhausts. Particle break-up and fragmentation mechanisms within the nozzle utilize a model based on the critical Weber number concept [Ref. 6]. However, test cases have indicated that assumptions made in the model yield unrealistic particle distributions [Ref. 7]. Very little experimental information is available that relates nozzle geometry and inlet particle size to the behavior of the particles as they pass through the nozzle. Light scattering techniques were not considered in obtaining particle sizes for Hermsen's data base, since they generally result in only D_{32} (volume-surface mean diameter) and are considered biased towards small particles. However, this technique has several distinct advantages. It is non-intrusive and theoretically can be used at any location in

or outside of the motor. Particle collection procedures and scanning electron microscope (SEM) evaluation can be used to determine the particle size distribution and, if this fits a log-probability function properly, the measured D_{32} can be directly related to D_{43} [Ref. 8].

This investigation was part of a larger ongoing effort at the Naval Postgraduate School. Its scope was (a) to develop and calibrate a diffractively scattered laser power apparatus, (b) to apply the technique at the entrance and exit of the exhaust nozzle of a small rocket motor, and (c) to obtain "across nozzle" particle size data from various propellants which can be used to validate or improve upon the existing particle size/behavior models used in the Air Force Improved Solid Performance Program (SPP).

II. DIFFRACTIVELY SCATTERED LIGHT METHOD

A. INTRODUCTION

The method has its origin in the Mie theory of light scattering by spherical particles. Gumprecht and Sliepcevich [Refs. 9 and 10] developed from this a theory describing the scattering properties of a polydispersion. Using this theory Chin, Sliepcevich, and Tribus [Ref. 11] conducted an investigation into the determination of particle size distributions in a polydispersion. This theory was limited to a small optical depth and there were limits on particle size and refractive index [Ref. 12]. A more general theory, applicable to finite optical depths, arbitrarily large particle size and arbitrary refractive index, was presented by Dobbins, Crocco and Glassman [Ref. 12]. However, their theory was applicable only to certain types of droplet size distributions. Roberts and Webb [Ref. 13] alleviated this problem and demonstrated the applicability of the "upper-limit distribution function" (ULDF) which was introduced by Mugele and Evans [Ref. 14]. Using the ULDF Roberts and Webb concluded that the volume-surface mean diameter, D_{32}, of a polydispersion could be accurately determined from the intensity of diffractively scattered light without any knowledge of the general distribution type. Dobbins and Jizmagian [Refs. 15 and 16] also concluded that the mean scattering cross section of

particles was primarily dependent on the mean diameter D_{32}, and only weakly dependent on the shape of the size distribution function when the refractive index is near unity. The ratio of scattered light at two forward angles was shown to be relatively insensitive to particle refractive index and concentration by Hodkinson [Ref. 17]. He also demonstrated that this ratio yields a measure of D_{32}.

With the above theories as a basis, experimental methods have been developed for estimating the volume-surface mean diameter, D_{32}, of a polydispersion of particles. Nejad et al [Ref. 18] used this method for measurement of the mean droplet diameter resulting from atomization of a transverse liquid jet in a supersonic airstream. Mean diameter, refractive index and volume concentration of aerosols have been determined by Powell et al [Ref. 19] using this technique in conjunction with light transmission measurements. More recently the practicality of this method for determination of particle sizes in the exhaust of a solid propellant rocket has been generally demonstrated by Karagounis [Ref. 20].

B. TECHNIQUE

The theory for the scattering of light by a single dielectric spherical particle of size number, α, gives the following expression for the radiant intensity $I(\theta)$ [Ref. 12]:

$$\frac{I(\theta)}{E_0} = \frac{D^2}{16}\left\{\alpha^2\left[\frac{2J_1(\alpha\theta)}{\alpha\theta}\right] + \left[\frac{4m^2}{(m^2-1)(m+1)}\right]^2 + 1\right\} \qquad (1)$$

where D is the diameter, α is the particle size number ($\pi D/\lambda$), λ is the wavelength of incident light, m is the refractive index of the scattering media, θ is the angle measured from the forward direction (radians) due to an incident planar wave of irradiance E_0 and J_1 is the Bessel function of first kind of order unity.

The three terms in the bracket of Equation (1) represent the Fraunhofer diffraction, the optical scattering due to refraction of the centrally transmitted ray and the optical scattering due to a grazingly incident ray, in that order. The following restrictions apply to Equation (1) [Ref. 12]:

(1) The incident light must be planar and monochromatic.

(2) The forward angle ϑ must be small ($\theta \cong \sin \vartheta$).

(3) The particle size number ($\alpha = \pi D/\lambda$), and phase shift ($o = 2\alpha(m-1)$) should be large.

(4) The distance between particle and observer should be large compared to D^2/λ.

(5) The particle must be non-absorbing.

Dobbins et al [Ref. 12] found that for a polydispersion, when the expression for intensity of scattering is normalized (by dividing by the intensity of diffractively scattered light in the forward direction ($\vartheta = 0$)), the second and third terms in Equation (1) were small and could be ignored. Thus, the expression for the normalized integrated intensity of forward scattered light, $I(\theta)$, due to a polydispersion of large particles is given as:

$$I(\theta) = \frac{\int_0^{D_\infty} \left[\frac{2J_1(\alpha\theta)}{\alpha\theta}\right]^2 N(D) D^4 dD}{\int_0^{D_\infty} N(D) D^4 dD} \tag{2}$$

where D_∞ is maximum diameter expected; and N(D) is a distribution function such that the integral of N(D) over the diameter interval is the probability of occurrence of particles within that interval. Equation (2) is valid when all particles are illuminated equally or when the attenuation of the incident beam is slight.

The transmission law for a polydispersion of particles is given by [Refs. 12, 15, and 21]:

$$\frac{E}{E_0} = e^{-\tau L} = \exp\left(-\frac{3}{2}\bar{Q}\, C_v L/D_{32}\right) \tag{3}$$

and by [Ref. 22]:

$$T = \frac{E}{E_0} = \exp\left(-\frac{3}{2}\bar{Q}\, C_m L/\rho D_{32}\right) \tag{4}$$

where $\bar{Q}$ is the average extinction coefficient; C_v and C_m are the volume and mass concentration of particles, respectively, τ, turbidity; L, path length, and ρ, particle density. $\bar{Q}$ and D_{32} are defined as [Ref. 22]:

$$\bar{Q} = \frac{\sum Q(D) N(D) D^2 \Delta D}{\sum N(D) D^2 \Delta D} \tag{5}$$

$$D_{32} = \frac{\sum N(D) D^3 \Delta D}{\sum N(D) D^2 \Delta D} \tag{6}$$

Dobbins [Ref. 12] recommends that the optical depth (τL) be maintained below 1.5 to prevent distortion of the illumination profile, $I(\theta)$ vs θ.

Using the ULDF developed by Mugele and Evans [Ref. 14], Roberts and Webb [Ref. 13] have concluded that a value of D_{32} may be determined from the intensity of diffractively scattered light from a polydispersion of spherical particles, for a wide range of size distributions. They developed a universal illumination profile (shown in Figure 5) which is a mean curve showing the relation between normalized intensity $I(\theta)$, and $\bar{\theta}$, a reduced angle of scattering equal to $\pi D_{32}\theta/\lambda$. Using this curve one can determine mean particle size but not the distribution of sizes.

The value of D_{32} may then be determined as follows.

(1) The optical apparatus is calibrated by using particles of known size as a scattering media, i.e. $I(\theta)$ vs $\bar{\theta}$ curves are generated and compared to the universal curve.

(2) The actual particles, in the current investigation the exhaust of the rocket motor, are introduced and $I(\theta)$ vs ϑ is determined.

(3) Knowing $I(\theta)$ and ϑ, $\bar{\vartheta}$ is determined from the calibration curve and/or the universal curve.

(4) D_{32} is determined using the relation:

$$D_{32} = \frac{\bar{\theta}\lambda}{\theta\pi} \tag{7}$$

C. APPLICABILITY

Karagounis [Ref. 20] has demonstrated the applicability of this technique in estimating the size of Al_2O_3 particles in the exhaust of a rocket motor. The restrictive conditions for the applicability of equation (2) were satisfied in the present experiment in a similar manner.

(1) A He-Ne laser with spatial filter and beam expander-collimator provided a planar, monochromatic light source.

(2) The forward angle θ was less than 6°.

(3) Large particle size number (>1) $\alpha = \pi D/\lambda$ was satisfied (with λ = .6328 μm, 0.2 μm < D < 20 μm, then $1 < \alpha < 100$).

(4) Large phase shift was provided (>1). (Estimating m = 1.76 for Al_2O_3 [Ref. 23] and $1 < \alpha < 100$, $1.52 < \rho < 152$.)

(5) The distance between the photodiode array and the particles was set at .8 m, which is considerably greater than D^2/λ = 632 μm (for a D_{max} of 20 μm).

(6) The final condition calling for non-absorbing particles is not met exactly, however the absorbing coefficient for Al_2O_3 is approximately 10^3 times smaller than the scattering coefficient for the wavelength, refractive index and size numbers considered here [Ref. 20]. Plass [Refs. 23-25] presents a very detailed discussion of this aspect.

The additional requirement of optical depth, $\tau L < 1.5$ is satisfied by not applying this technique to situations where $E/E_0 < 0.25$ (Eq. 4).

III. EXPERIMENTAL APPARATUS

A. LIGHT SCATTERING APPARATUS

A schematic diagram of the final optical set-up is shown in Figure 1 and photographs are shown in Figure 2. A schematic of the Data Acquisition System is shown in Figure 3. The instruments and optical equipment are listed in Table I. A complete description of the Data Acquisition System is presented in Reference 26. The optical equipment was mounted on two parallel optical benches, one for the beam passing through the exhaust and one for the beam passing through the motor at the nozzle entrance. Initially a 5 mw Helium-Neon laser was used as the light source. This was later replaced by a 10 mw Argon laser, for reasons to be discussed later. A spatial filter/beam expander located directly in front of the light source produced a uniform light beam, one centimeter in diameter. Initially a pinhole with a 2.2 mm diameter was located in front of the collimating apparatus. This pinhole was used to reduce the size of the laser beam in order to decrease the measurement volume. Further experimentation eventually determined that this pinhole was not necessary. The intensity of the beam was decreased using a 1 percent neutral density filter to prevent saturation of the linear photodiode arrays. The beam was split using a 50/50 cube beam splitter. One beam continued through the

exhaust, the other traveled to a 90 degree prism where it was turned parallel to the first beam and directed through the motor at the nozzle entrance. Passage of the beam through the motor was afforded by mounting circular glass windows in the walls of the motor on either side of nozzle entrance area. Both beams were passed through identical condensing lenses (5 cm in diameter with focal lengths of 500 mm) and focused on linear photodiode arrays. The photodiode array assemblies each consisted of a linear photodiode array, a "mother board" circuit card and an array board. Each assembly was mounted in a lighttight black box fitted with a narrow band pass filter. Each box was mounted on two translation stages to provide vertical and horizontal degrees of freedom. The linear photodiode array was a self-scanning photodiode array consisting of 1024 silicon photodiodes mounted in a vertical row on 25 μm centers. The aperture width was 26 μm. The circuits provided an integrated, sampled-and-held output. The "mother board" contained most of the circuitry, including the driver/amplifier, clock, start, and end of scan functions. The array board contained only the circuitry which must be located close to the array itself. The output signal was passed through a variable low pass filter (for reasons discussed later) before transmission to the data acquisition system. The reading of the array was accomplished in 36 milliseconds, which corresponds to a rate of 30 kHz.

B. ROCKET MOTOR

The motor was cylindrical, stainless steel with a copper nozzle. The chamber was two inches in diameter and two inches deep (Figure 4a). The nozzle throat diameter was .245 inches (for a chamber pressure of 760 psi). An internally burning, six-pointed star (Figure 4b) was selected for the grain design in an effort to achieve a period of steady state pressure in which to take data. The grains were one inch long and two inches in diameter with a web thickness of 0.5 inches. Each grain was cut out manually from a one inch thick slab of propellant using frabicated shaped cutters. The grains were prepared for ignition by applying a thin black powder and glue mixture to the inner surface of the grain. Electrically ignited $BKNO_3$ was discharged from the head end of the motor onto the inner surface of the grain, thus igniting the black powder, which in turn ignited the propellant. A cylindrical stainless steel tube (8" O.D.) was mounted at the exhaust of the motor to collect the samples of exhaust particles for SEM evaluation.

Two circular windows were mounted in the walls of the motor on either side of the nozzle entrance area. The windows were recessed from the motor chamber. To keep the windows clean, nitrogen was discharged into this recessed area and evenly diffused through a sintered metal filter (Figure 4c).

IV. EXPERIMENTAL PROCEDURE

The apparatus was established in an open test cell of the Combustion Laboratory. The output signal of the system contained a quantity of high frequency noise. After numerous unsuccessful attempts to locate and eliminate the source of this noise, it was decided to use a variable low pass filter to eliminate the noise from the output signal. Subsequent examination of the filter effects during the calibration runs determined that the filter did not adversely affect the accuracy of the data readings. After a collimated and filtered beam was acquired, the focus was set 1.52 mm above the first diode of the array. Care was taken at all times to avoid focusing the beam directly on the diodes to prevent damage to the array. It was also found necessary to slightly cant the focusing lens to prevent interference from reflected light.

Next, the accuracy of the Diffractively Scattered Light Method (DSLM) for obtaining the mean diameter of particles was investigated. A comparison was made between experimentally determined normalized intensity ($I(\theta)$) versus non-dimensional angle ($\bar{\theta}$) profiles and the "universal" theoretical profile (Figure 5). The various profiles were first obtained using spherical glass beads of different size ranges. The individual profiles for the three size ranges of beads (1-37 μm, 37-44 μm and 53-63 μm) are shown in Figures 6-8.

The profiles for each size range were determined by suspending the particles in water contained in a Plexiglas box (2.5" x 3.0" x 2.5"). Suspension was maintained using a magnetic stirrer. The first step in this calibration procedure was to obtain the zero-scattering profile, that is, the light intensity on each diode after passage through the stirred water, before particles were introduced. Next the particles were introduced and the intensity reading at each diode was taken. Examples of intensity versus diode at 1 and 3 kHz filter settings are shown in Figures 9 and 10, respectively. The analog to digital conversion was accomplished by the data acquisition system. (A complete discussion and listing of the data acquisition and the reduction procedures discussed below are presented separately by Hansen [Ref. 26].)

After obtaining the two scattering profiles the normalized intensity $I(\vartheta)$ versus angle theta (θ) profile was determined according to the relation:

$$I(\vartheta) = \frac{I_{\vartheta,p} - I_{\vartheta,o}}{I_{cl,p} - I_{cl,o}} = \frac{V_{\vartheta,p} - V_{\vartheta,o}}{V_{cl,p} - V_{cl,o}} \qquad (8)$$

where I_{cl} or V_{cl} are the projected light intensity and related voltage at the centerline, and I_{ϑ} and V_{ϑ} are the light intensity and voltage at an angle, ϑ (Figure 11). "o" and "p" symbolize no particles and with particles, respectively. The first step in determining the normalized intensity was to calculate the numerator, ΔV_{ϑ}, of equation (8) by subtracting

the two voltages at corresponding diode numbers. The maximum difference (lower limit on diode number) computed was taken as the point where the diffractively scattered light intensity was dominant over the transmitted light intensity. The computer determined the diode number where this occurred. An upper limit on diode number was taken near the point where $V_{\theta,p} - V_{\theta,o}$ first became zero (Figure 10). A least squares linear fit was then made to the ΔV_θ vs diode number data and extrapolated to obtain $V_{cl,p} - V_{cl,o}$ (the forward scattered light at $\theta = 0$). $I(\theta)$ vs θ could then be calculated (equation (8)).

An example of the relationship of $I(\theta)$ versus θ thus produced is shown in Figure 12. At this point the relationship of $I(\theta)$ versus $\bar{\theta}$ is determined using the relationship:

$$\bar{\theta} = \frac{\pi D_{32}}{\lambda} \theta \qquad (9)$$

where D_{32} is the mean diameter of the particle range being used in the calibration. $I(\theta)$ vs $\bar{\theta}$ can then be plotted (Figure 13). An nth order polynomial curve fit was then applied to the data over a user specified range. The order of the polynomial (also user specified) may be varied from 1 to 10 depending on the appearance of the data. The range corresponded to the range of the diodes selected for determination of the centerline values as mentioned above. An example of the result of this process is shown in Figure 13. The

resulting curve is then plotted on a semi-log scale for comparison with the universal curve (Figures 5-8).

The results shown in Figures 5-8 for glass spheres generally agree with those of Karagounis [Ref. 20] in that larger deviations from the universal curve occur as $\overline{\theta}$ increases (beyond $\overline{\theta} = 2.5$). However, unlike the data of Karagounis, agreement with the universal curve was not dependent on particle mean diameter.

Several possible causes for this lack of agreement were investigated. First the effect of filter setting was checked. Keeping all other variables constant, data were taken with 1 kHz and 3 kHz filter settings. The resultant profiles shown in Figure 14 are almost identical. Next the effect of horizontal displacement of the array was studied. Again keeping all other variables constant, two runs were made. The first had the focal point centered on the axis of the array. In the second, the focal point was displaced to one side just far enough to minimize non-uniform intensity variations. Again the results showed little difference from one another (Figure 15). A narrower particle suspension box was also used to decrease the depth of the field, but it likewise showed little change from the profile using the wider box. Signal-to-noise ratio and dark current were two factors which could not be completely eliminated and may contribute to the lack of agreement at higher $\overline{\theta}$.

Using the same procedure as discussed above, $I(\theta)$ versus $\overline{\theta}$ profiles were prepared for four size ranges of non-spherical Al_2O_3 powder. The results are shown in Figure 16. The results indicate reasonable agreement with the universal curve. The experimental profiles had greater slopes than the theoretical profile as they did for the spherical glass beads. However, for the Al_2O_3 the mean size affected the profile.

The particle size measuring technique was then applied to actual motor firings. Before each motor firing calibration of the recording equipment was conducted. Proper positioning of the laser beam on the array was verified. Then the zero scattering profile was recorded. The motor was fired and the scattering profile was recorded automatically at a specified pressure. Chamber pressure was recorded on a visicorder oscillograph. In the same manner previously described the normalized intensity ($I(\theta)$) versus angle (θ) was determined. D_{32} values were then calculated over the recorded $\overline{\theta}$ range, using both calibration curves and the universal curve, from the relation:

$$D_{32} = \frac{\overline{\theta}\lambda}{\theta\pi} \qquad (10)$$

Residue from the motor exhaust was captured in a stainless steel collection tube. Some of it was dissolved in acetone, subjected to an ultrasonic vibrator, allowed to settle and then dried in a vacuum oven. This "cleaned"

sample and an "as collected" sample were examined with an SEM. Photographs are shown in Figures 17 and 18.

V. RESULTS AND DISCUSSION

The original goals of this investigation were (a) to develop an apparatus to determine D_{32} from measurements of the diffractively scattered laser power spectra using rapid scans of linear photodiode arrays, (b) to apply the apparatus at the nozzle exit and through the motor at the exhaust nozzle entrance of a solid propellant rocket motor, and (c) to obtain "across-nozzle" particle data for comparison with the existing models for two-phase flow phenomena in exhaust nozzles. The first two goals were met, however, due to experimental difficulties the last goal was only partially achieved.

The apparatus developed for this investigation has been discussed above. Considerable difficulty was encountered during the initial set-up of the computer controlled data acquisition and data reduction procedures. The resulting experimental procedures have also been discussed above (Section IV). When the apparatus was applied to actual motor firings several additional difficulties occurred. These will be discussed below.

Keeping the windows clear without affecting either motor flow or the combustion processes presented the greatest challenge. The final solution (Figure 4c) consisted of a sintered metal filter to evenly diffuse the nitrogen into the window purge area and a converging nozzle tc slightly

accelerate the nitrogen flow into the motor. This system worked very well at all pressures investigated.

The light generated during the combustion process within the motor (but not at the nozzle exit) was found to produce significant radiation at the wavelength of the He-Ne laser (.6328 μm) initially used as the light source. This prohibited the measurement of any scattered light from the particles. The light source was changed to an argon laser (.4880 μm) and the problem was alleviated.

The location of the laser beam in the exhaust jet was found to be critical. If directed too far to the rear of the nozzle exit, it either missed the jet entirely due to the deflection of the jet or the particle number density was too low. Both problems resulted in a particle scattering profile that was nearly identical to the zero particle scattering profile. With the current motor the beam was located three inches to the rear of the nozzle exit.

The tests conducted are summarized in Table II. The first series of tests was conducted at 775 psia. There were two significant results: (1) there was insufficient light through the motor to get a scattering profile; (2) the measured D_{32} in the exhaust was large (30-50 μm). The photographs in Figures 17 and 18 show the apparent reason for this large D_{32} to be the presence of a small number of large irregularly shaped agglomerates, which were not Al or Al_2O_3 (typically ½-5 μm spheres). These agglomerates were most

probably inhibitor or binder char. Their influence was significant, as even a very few large particles greatly increase the measured D_{32}. The sensitivity of the technique to irregularly shaped particles has already been demonstrated (Figure 16). Repeated tests resulted in different D_{32} at the nozzle exhaust, apparently from different sizes of char agglomerates at the time the diode scan was made.

The tests made at approximately 500 psia (runs 3, 4 and 5, Table II) were made to determine, (1) if the size of the exhaust char agglomerates were sensitive to combustion pressure, and (2) if the lower chamber pressure would permit measurement of scattered light through the motor. In addition, repeated runs were made to acquire the diode data at different times during the run to determine whether the data was significantly time dependent. It was found that data could be obtained through the motor. Comparisons with the universal curve and the small glass bead calibration curve (Figure 6) yielded reasonable values for D_{32} of 16 and 12 μm, respectively. It was further determined that D_{32} measured at the nozzle exit was sensitive to burn time, as shown by the increasing values of D_{32} with increased time. And finally, as shown in Figure 17, the spherical Al/Al_2O_3 particles were still in the ½ to 5 μm size range. Therefore, the change in measured D_{32} was apparently due to changes in char agglomerate size during the run.

In run 6 an end burning grain was used in an attempt to reduce or eliminate the large char agglomerates. The results were: (1) a significant reduction in measured D_{32} (however, it was still larger than the Al/Al_2O_3 spheres), and (2) the larger optical path with particles (increased optical density) precluded the measurement of any scattering data.

VI. CONCLUSIONS

The technique developed for determining the change in D_{32} across a solid propellant rocket motor exhaust nozzle appears to work well. Additional effort is required to find a grain configuration and/or an inhibitor that minimizes the size of, or eliminates entirely, the char agglomerates. This is required in order to be able to obtain "across nozzle" data during a single test. This would allow realization of the final goal, that is, to obtain data for the validation of the two-phase flow models.

TABLE I

EXPERIMENTAL APPARATUS

1. Spectra Physics Model 147, Helium-Neon Laser. Power 5 mW, Random Polarization.

2. Power Supply for above, Model 247, 30 watts.

3. Laser Beam Expander with spatial filtering, 22 mm aperture, Oriel, Model 1526.

4. Plano-convex lens, 5 cm diameter. 50 cm focal length. (2)

5. Neutral density filter, FNG-043, 1%, 2.0 O.D.

6. Cube Beam-Splitter, 50/50.

7. 90° Prism.

8. Linear Photodiode Array, EG&G Reticon, G series, 1024 elements. (2)

9. Mother Board Circuit Card, EG&G Reticon, RC100B. (2)

10. Array Circuit Card, EG&G Reticon, RC106. (2)

11. Narrow Band Pass Filter. (2)

12. DC Power Supply for Photodiode Assembly.

13. Variable Low Pass Filter, Krohn-Hite, model 3343.

TABLE II: DATA SUMMARY

Propellant contained 2% by weight of Al (40 μm)

Run	1	2	3	4	4a (Nozzle Entrance)	5	6*
Date	15 Sep 82	19 Sep 82	21 Sep 82	23 Sep 82	23 Sep 82	24 Sep 82	25 Sep 82
Maximum Pressure (psia)	775	775	555	565	565	495	455
Readings Taken (psia) (see fig. below)	760 (b)	760 (b)	395 (a)	545 (b)	545 (b)	465 (c)	415 (c)
D_{32} Average, Universal Curve (μm)	52	39	24	37	16	56	16
D_{32} Average Calibration Curve Comparison (μm)**	38 m	30 m	20 s	30 s	12 s	40 ℓ	13 s

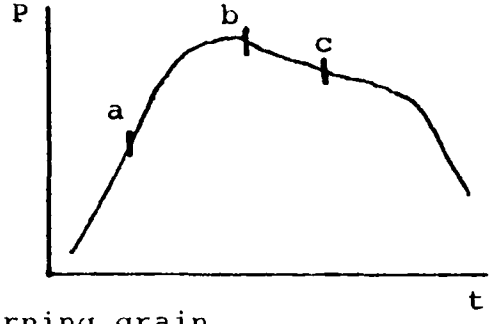

(Sample pressure-time trace showing points where data was taken)

*End-burning grain

**s--small particle calib.
m--medium particle calib.
ℓ--large particle calib.

Figure 5

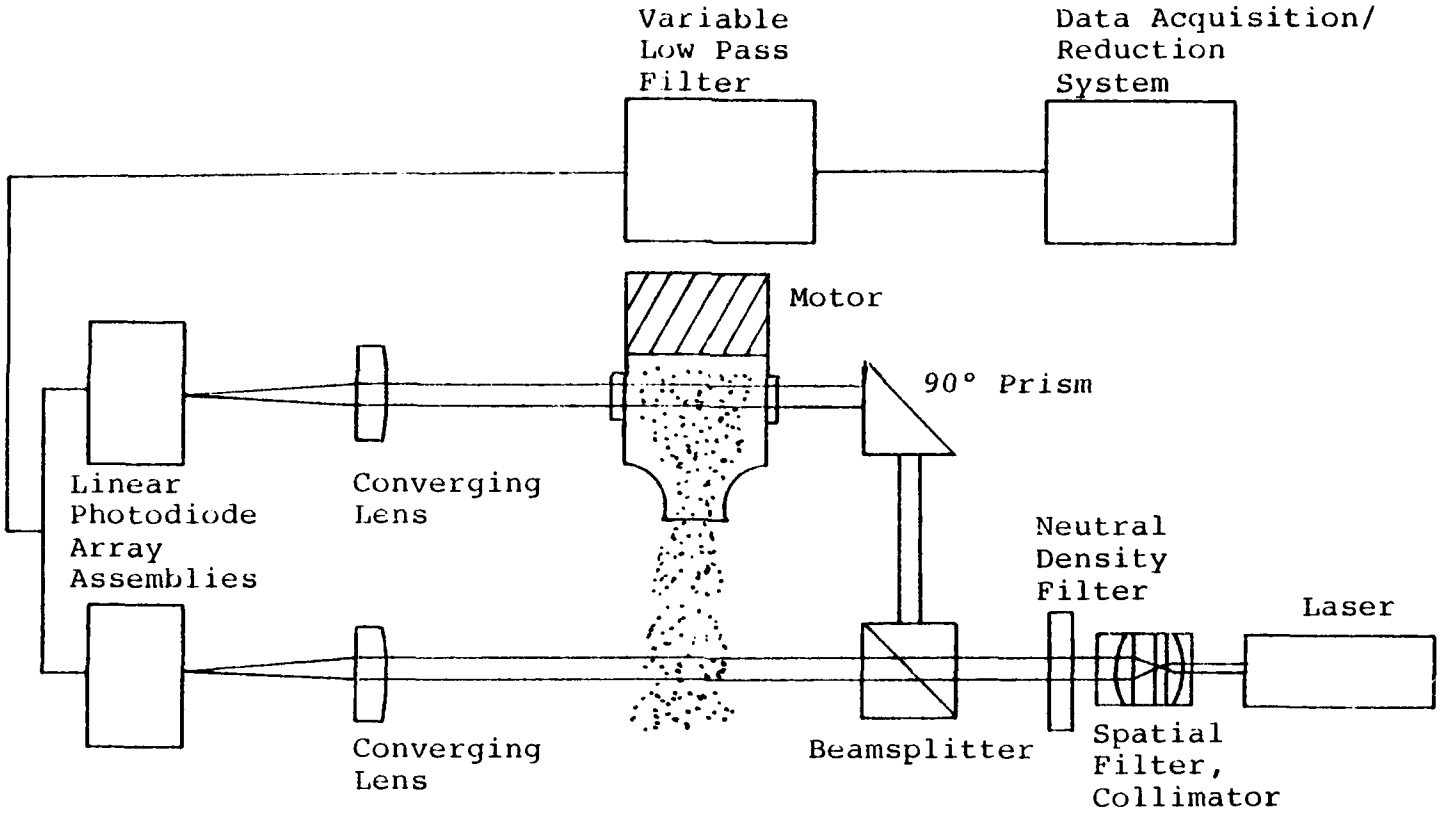

Figure 1: Schematic Diagram of Diffractively Scattered Light Apparatus

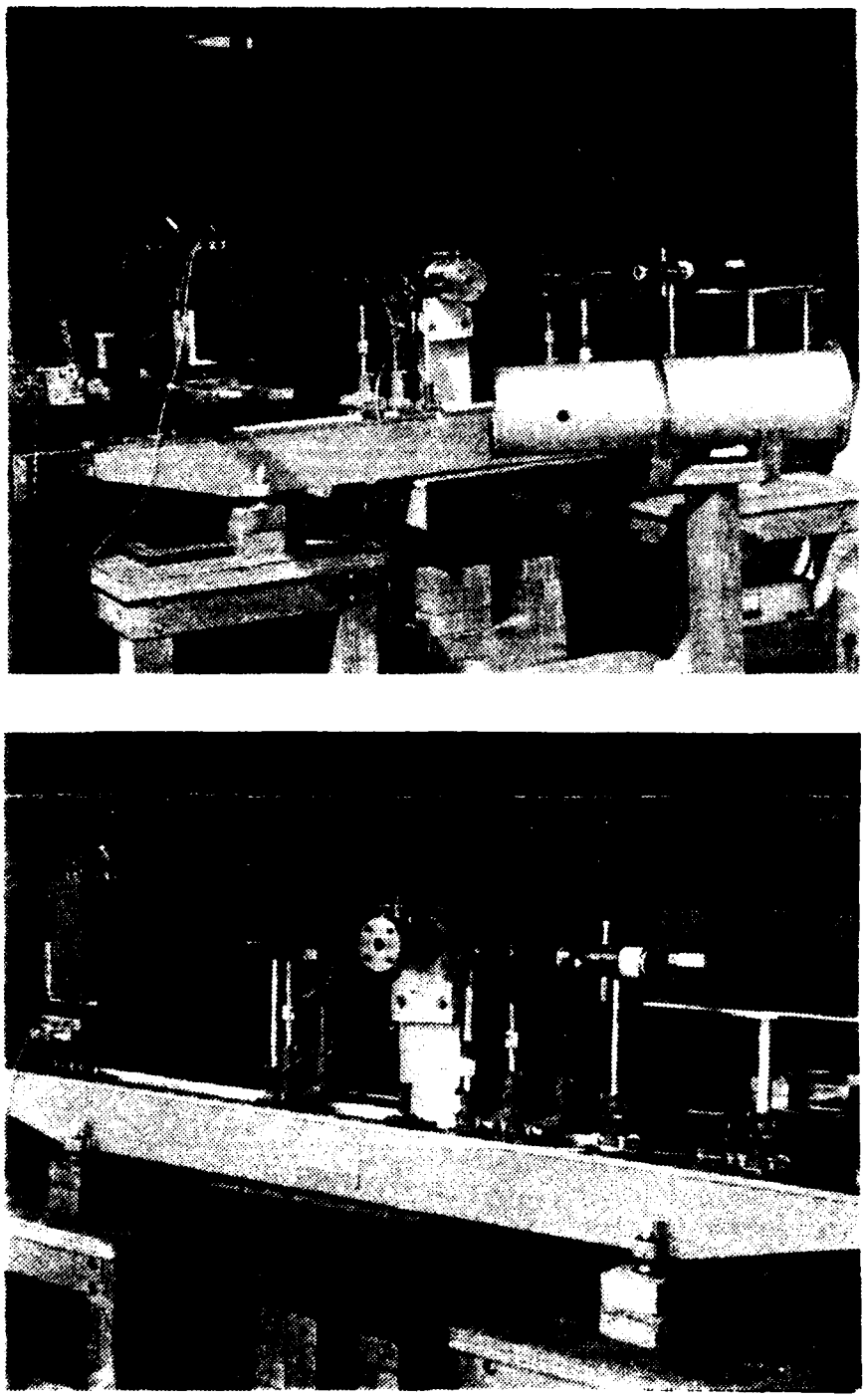

Figure 2: Photographs of Light Scattering Apparatus

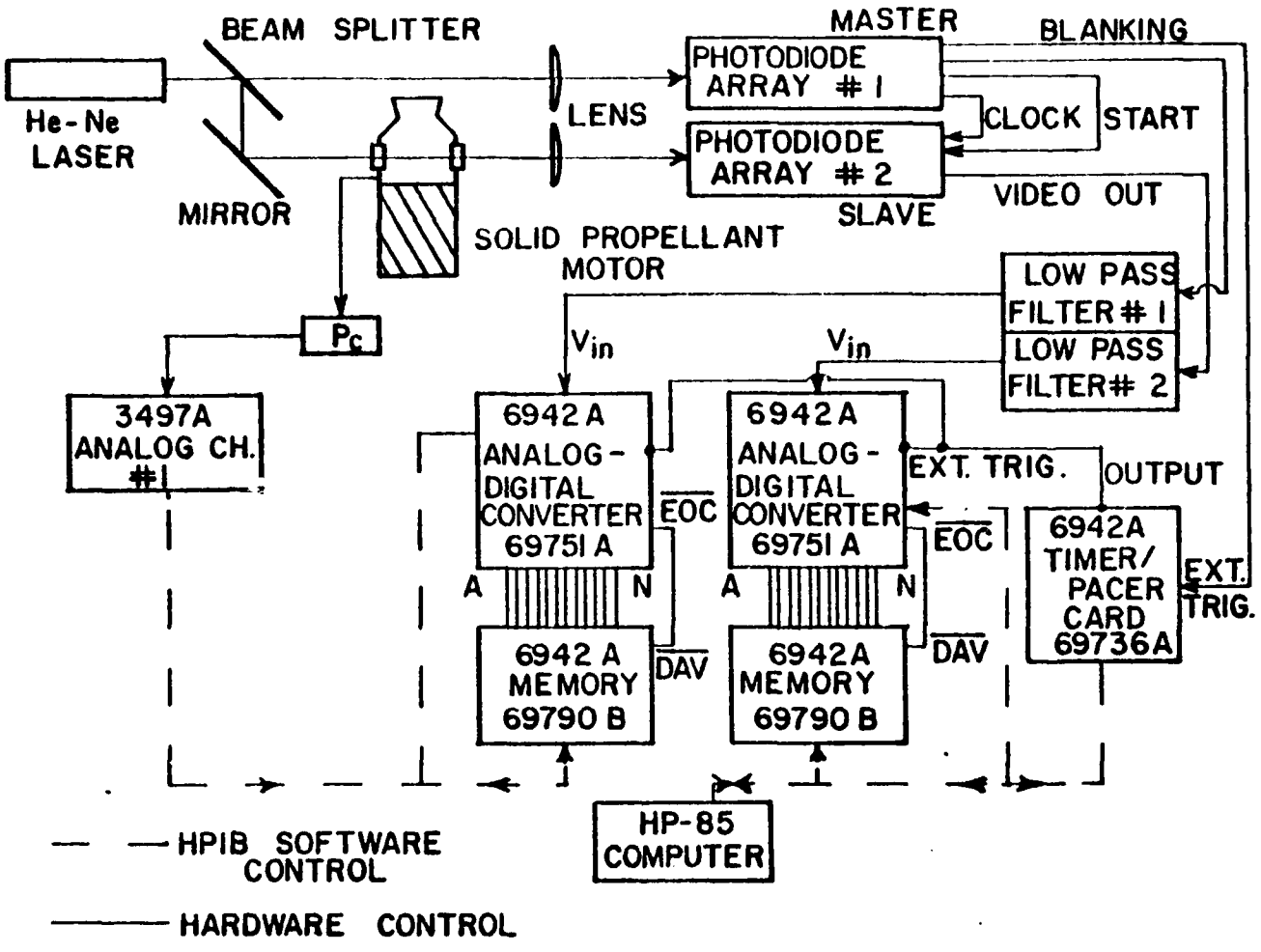

Figure 3: Schematic of Data Acquisition System

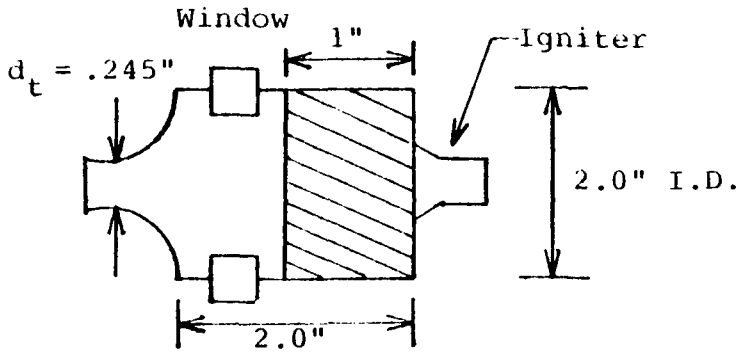

(a) Motor

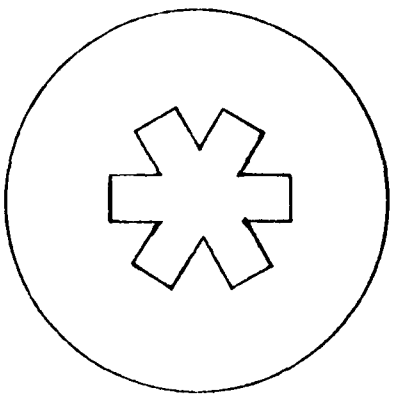

(b) Grain Design, End-view
(Actual Size)

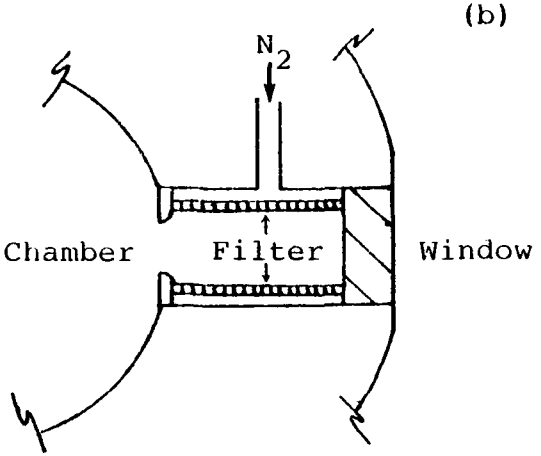

(c) N_2 Purge System
(Side View)

Figure 4: Motor Components

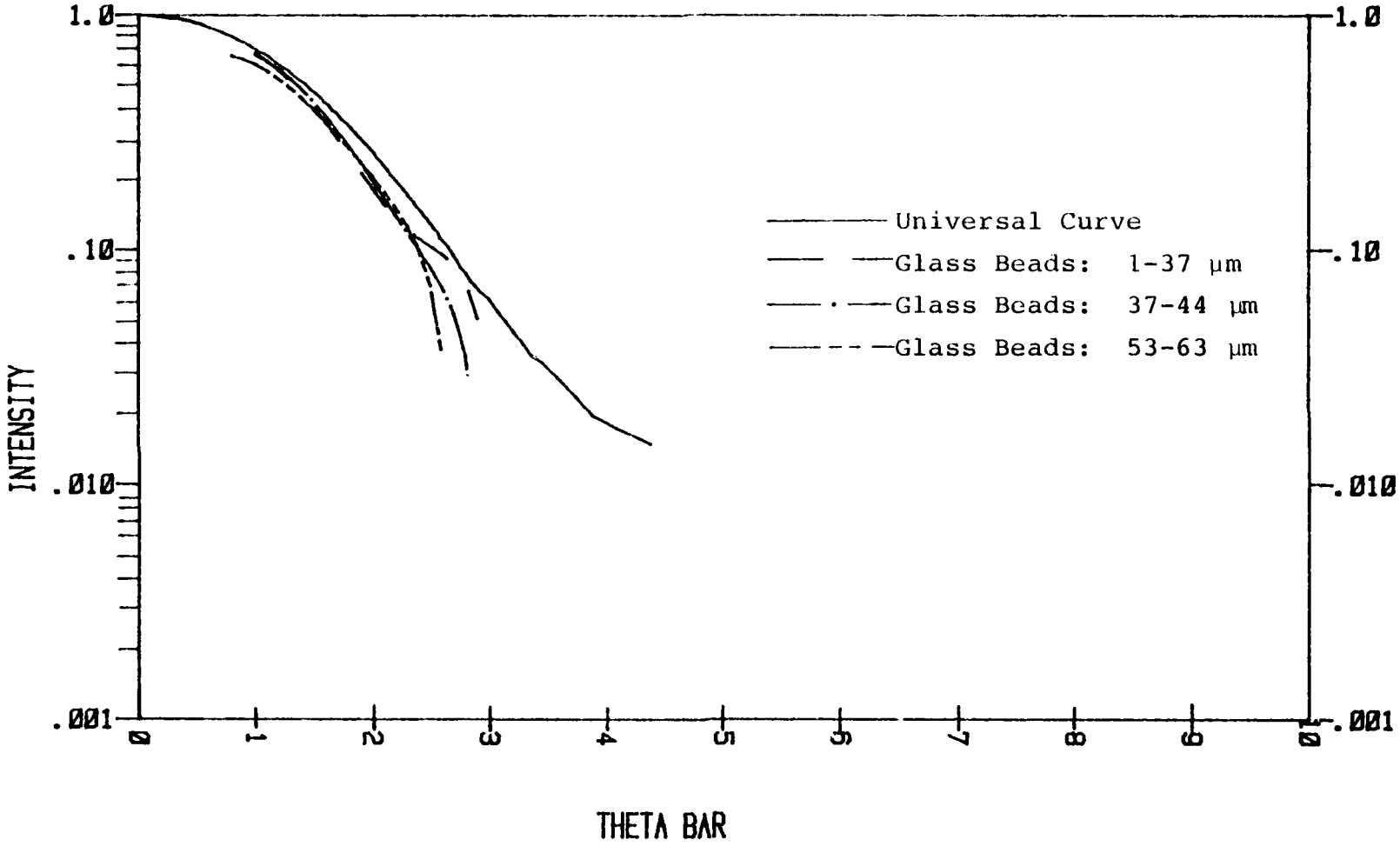

Figure 5: $I(\theta)$ vs $\bar{\theta}$, Normalized Intensity Profiles, Spherical Glass Beads

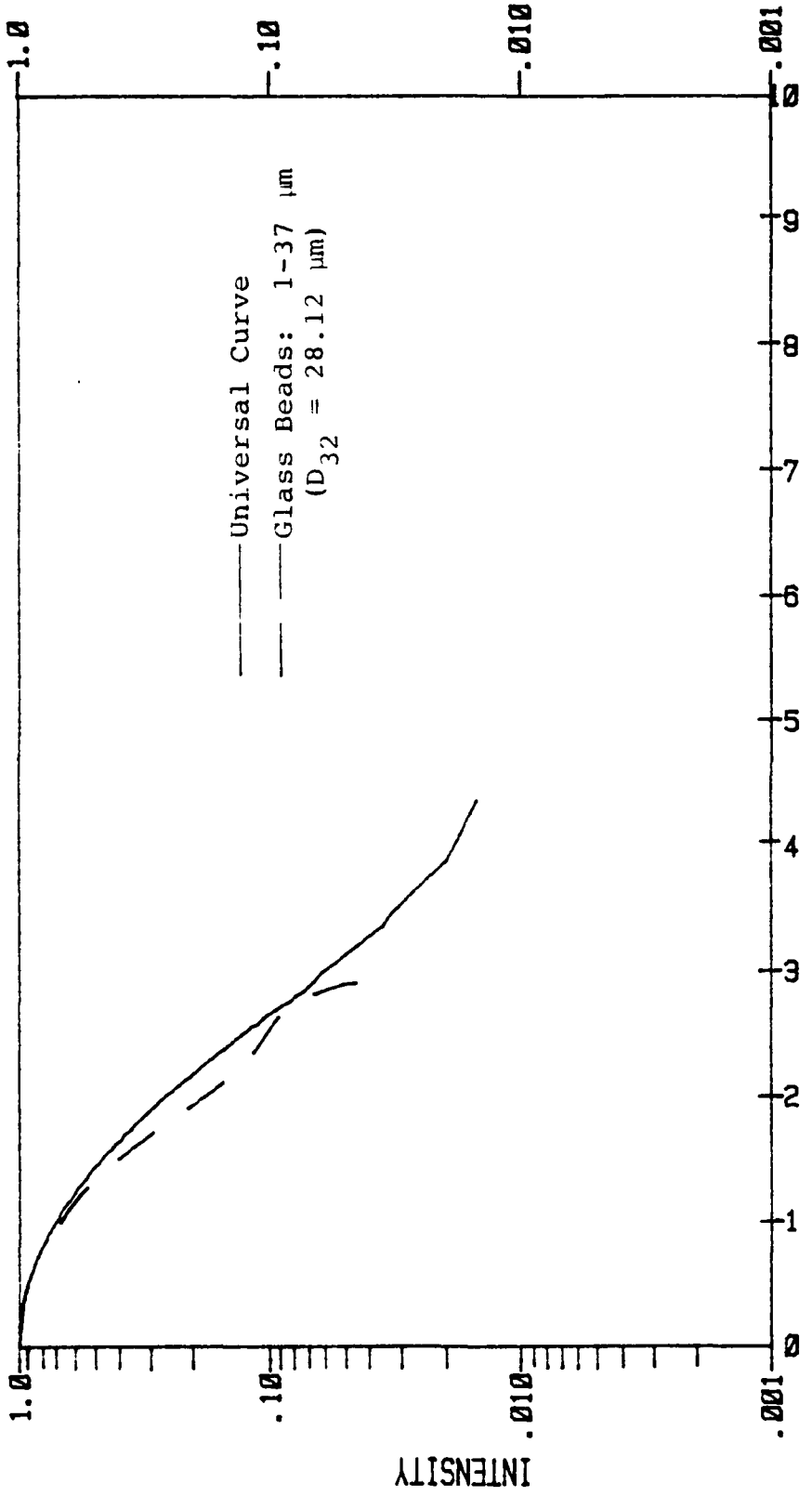

Figure 6: $I(\theta)$ vs $\bar{\theta}$; Spherical Glass Beads, 1-37 μm

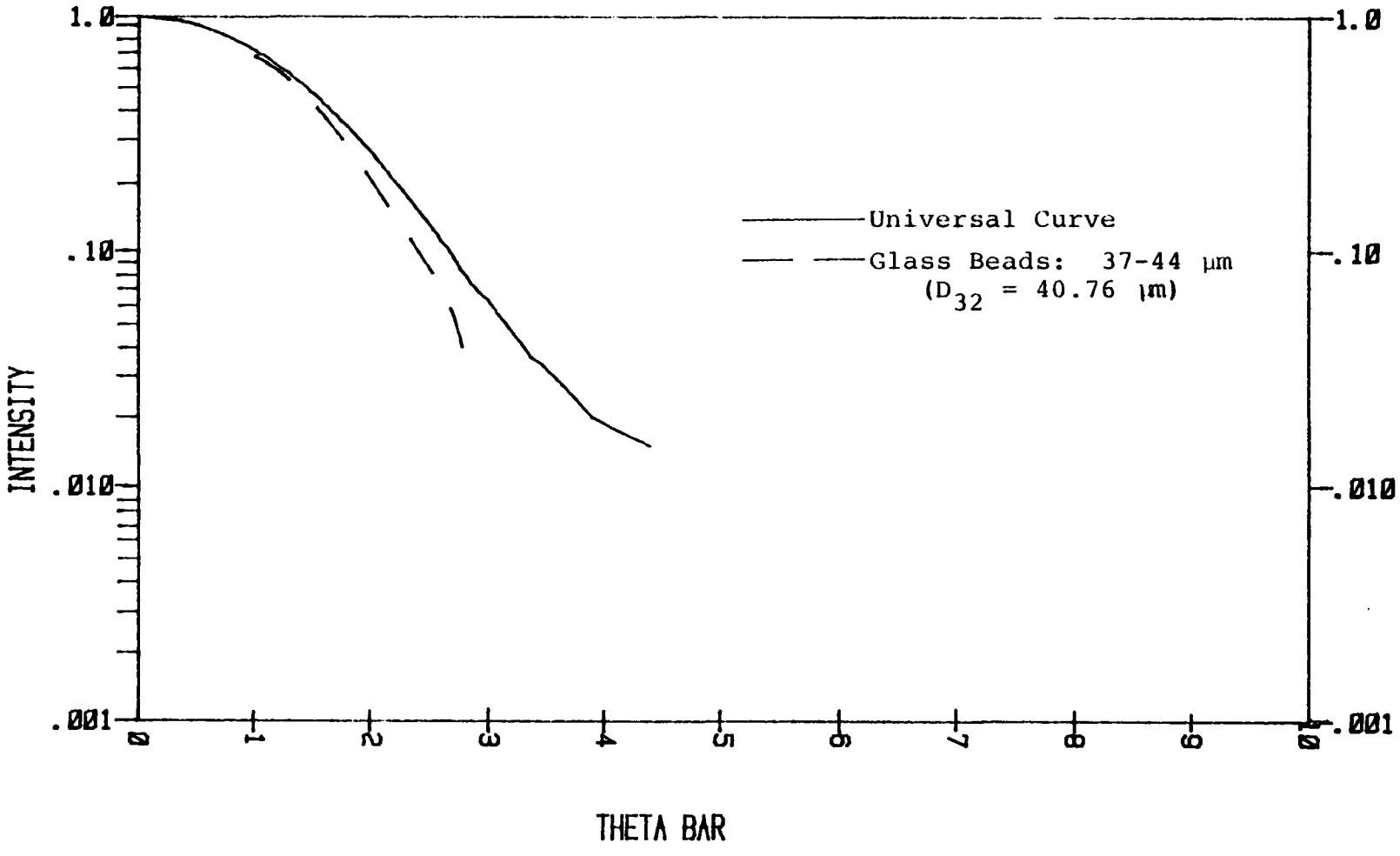

Figure 7: I(θ) vs $\bar{\theta}$; Spherical Glass Beads, 37-44 μm

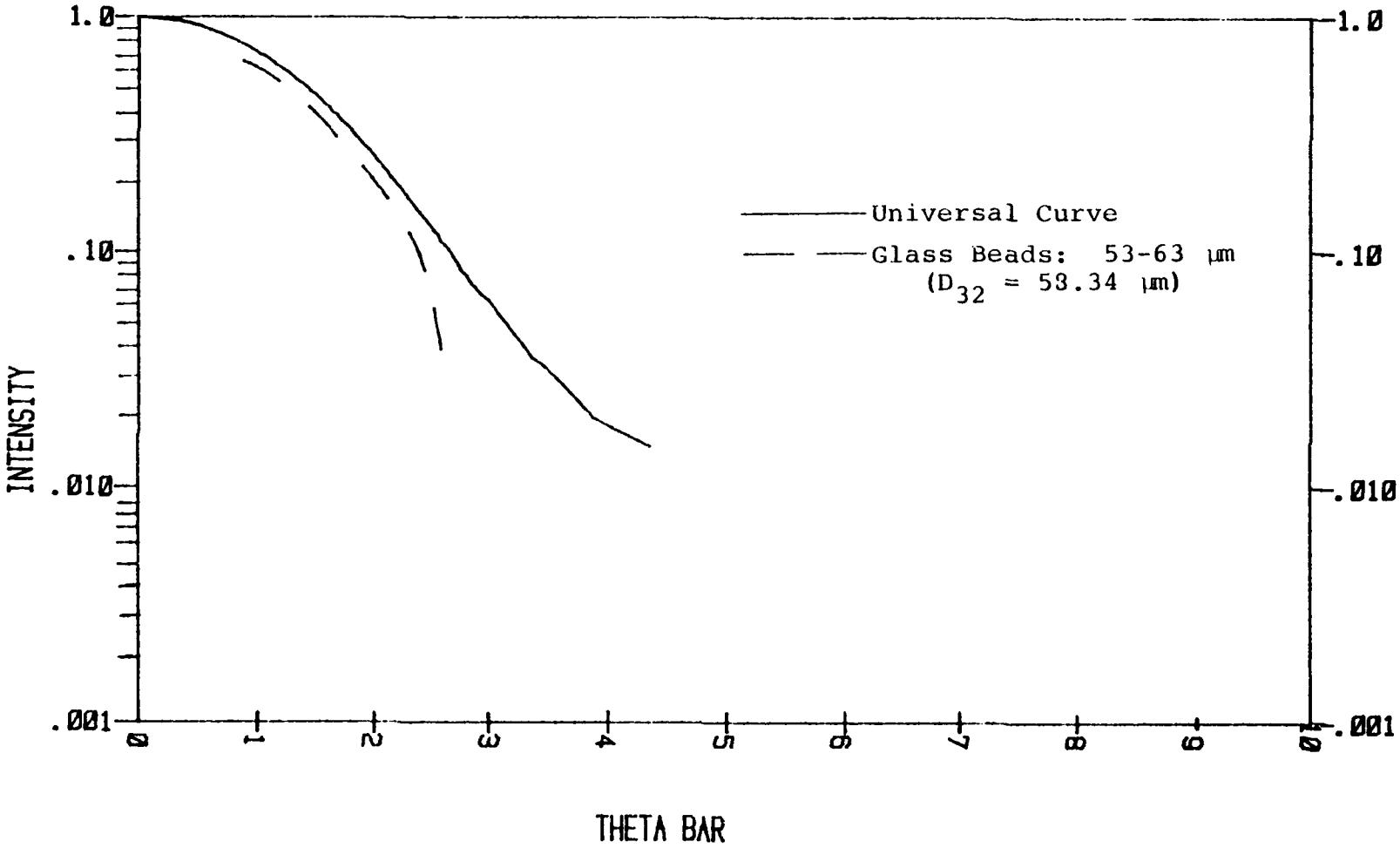

Figure 8: $I(\theta)$ vs $\bar{\theta}$; Spherical Glass Beads, 53-63 μm

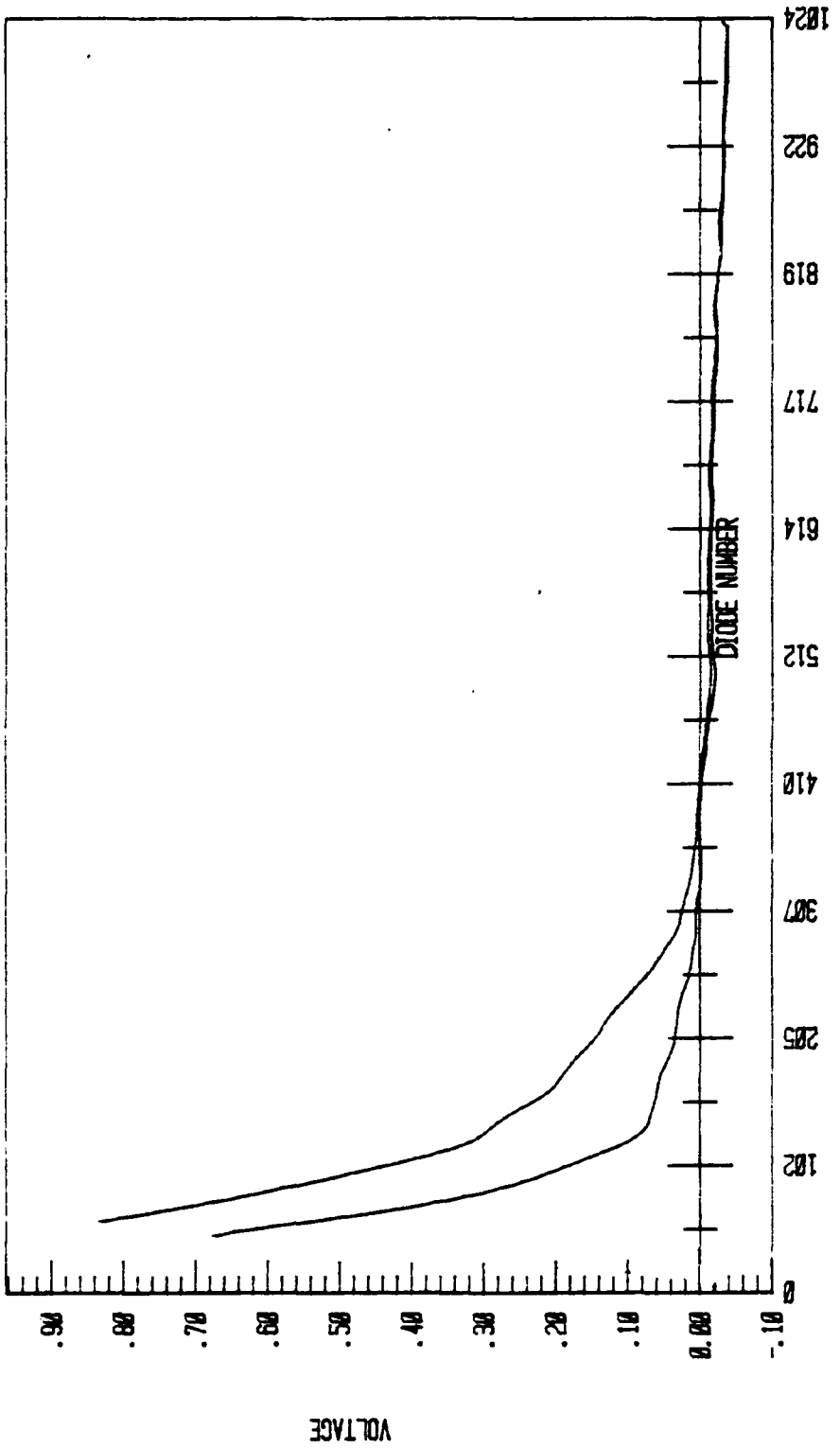

Figure 9: Voltage vs Diode--1 kHz Filter

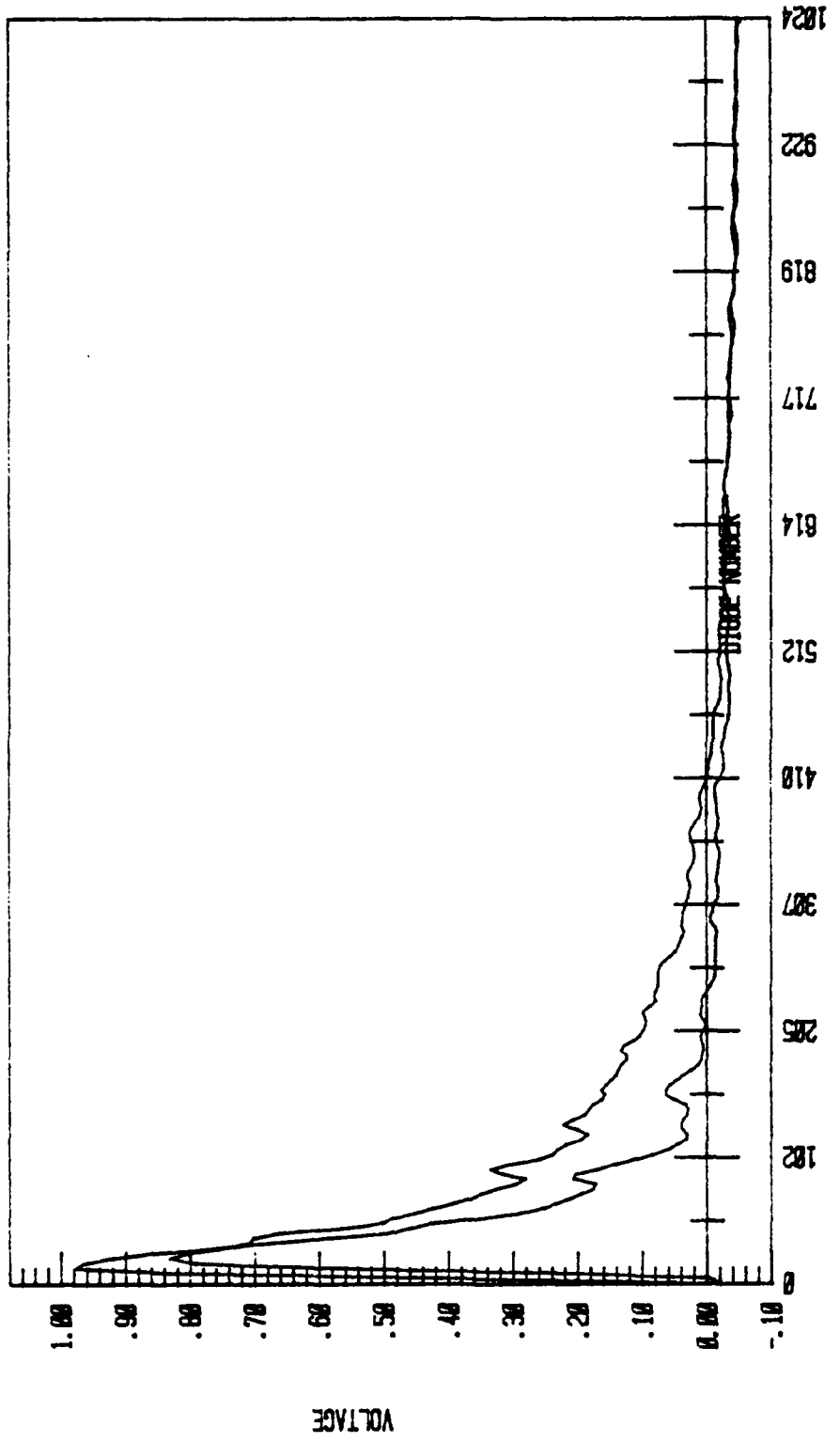

Figure 10: Voltage vs Diode--3 kHz Filter

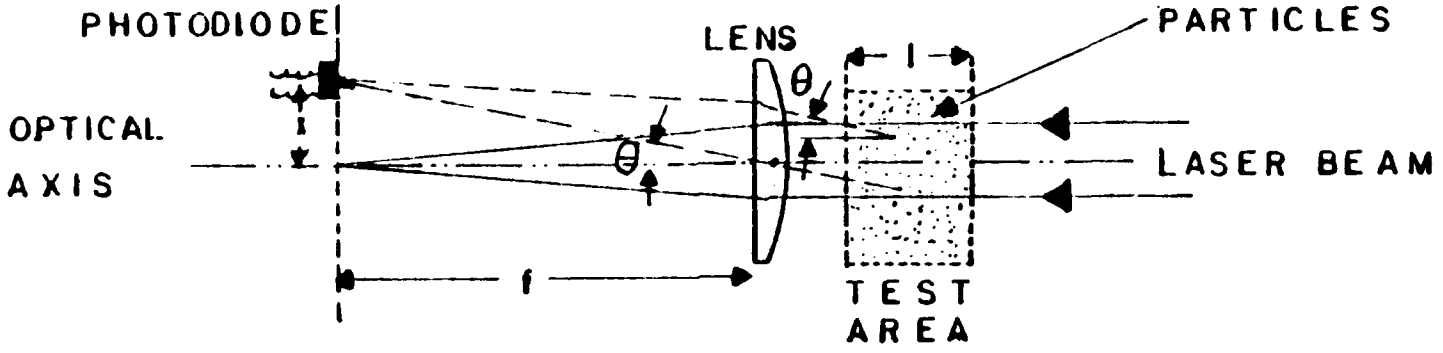

For air: $\theta \cong \frac{x}{f}$

For water: $\theta \cong \frac{x}{f \cdot m}$, m = 1.35, refractive index of water [Ref. 9]

Figure 11: Light Scattering Geometry

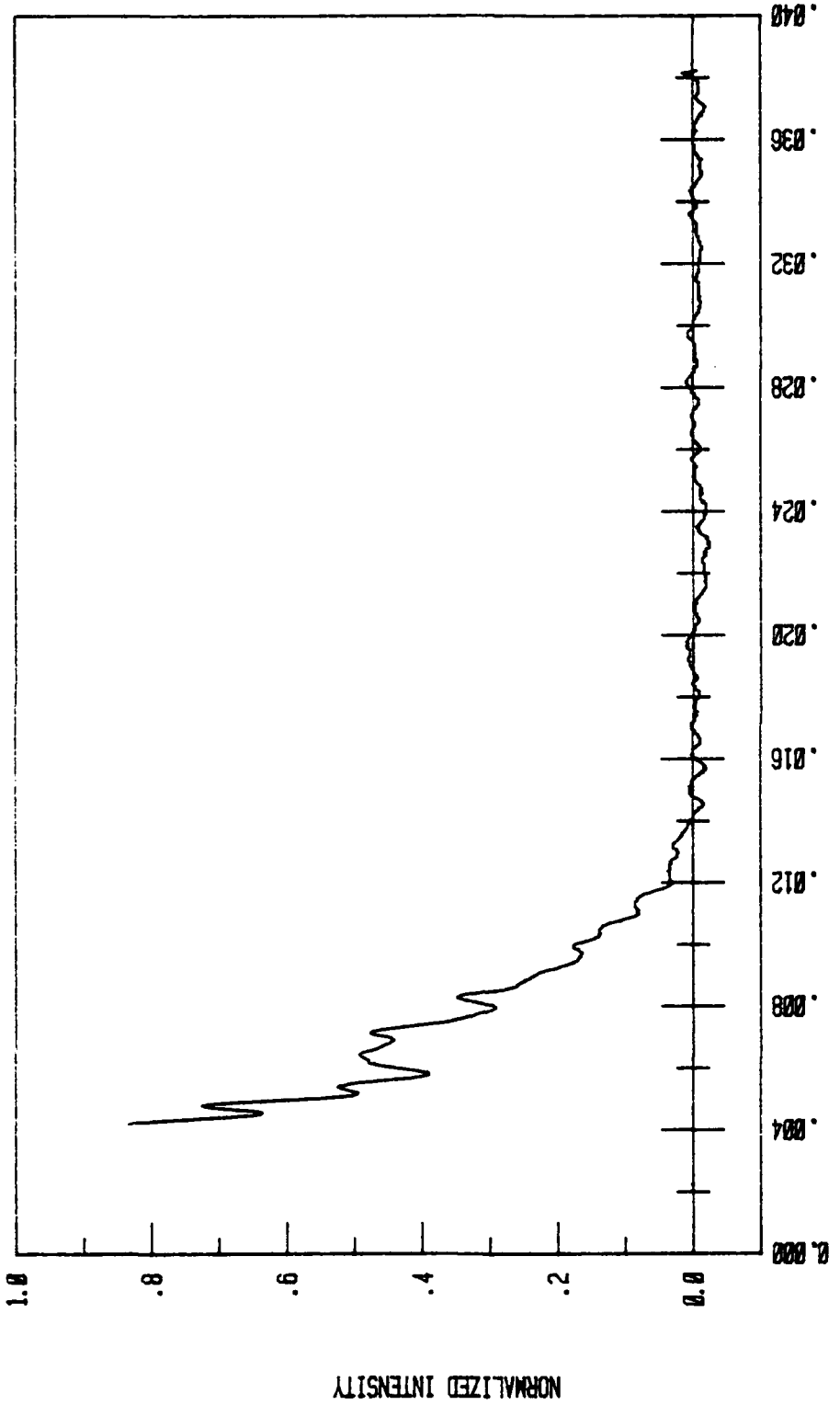

Figure 12: I(θ) vs θ--Example

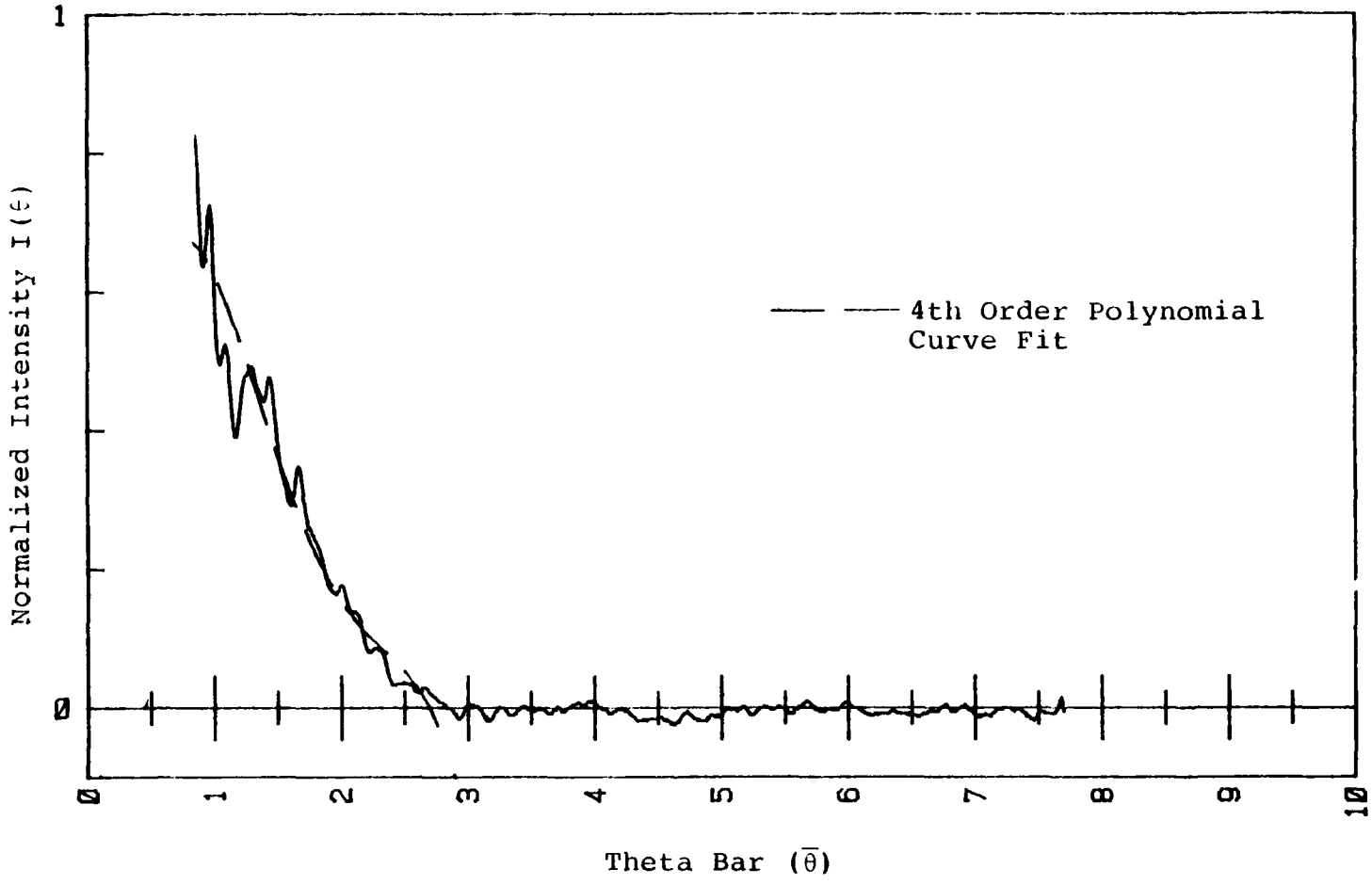

Figure 13: $I(\theta)$ vs $\bar{\theta}$--Example

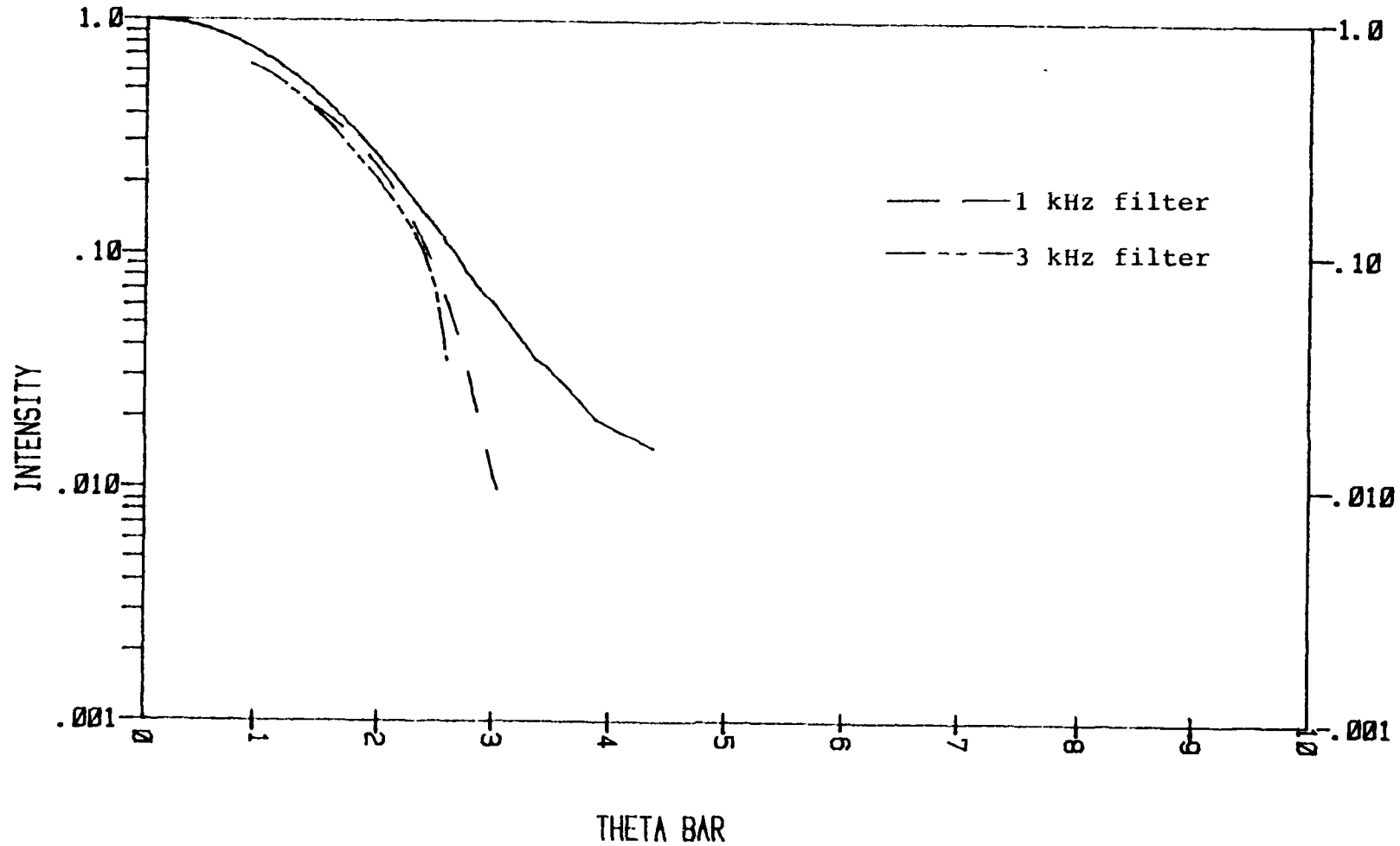

Figure 14: I(θ) vs $\bar{\theta}$--1 and 3 kHz Frequency Filter Settings

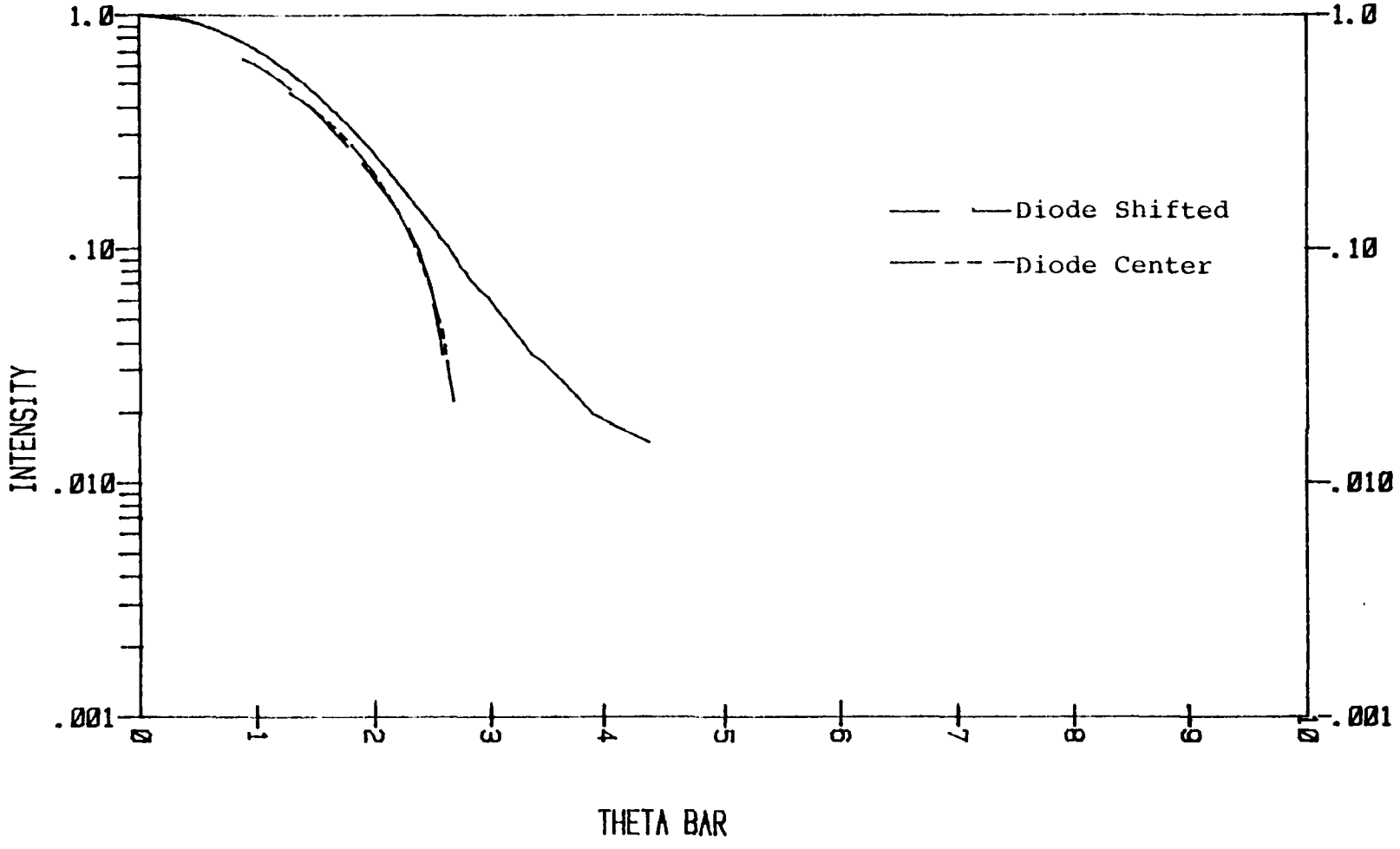

Figure 15: I(θ) vs $\bar{\theta}$--Horizontal Displacement of Array Comparison

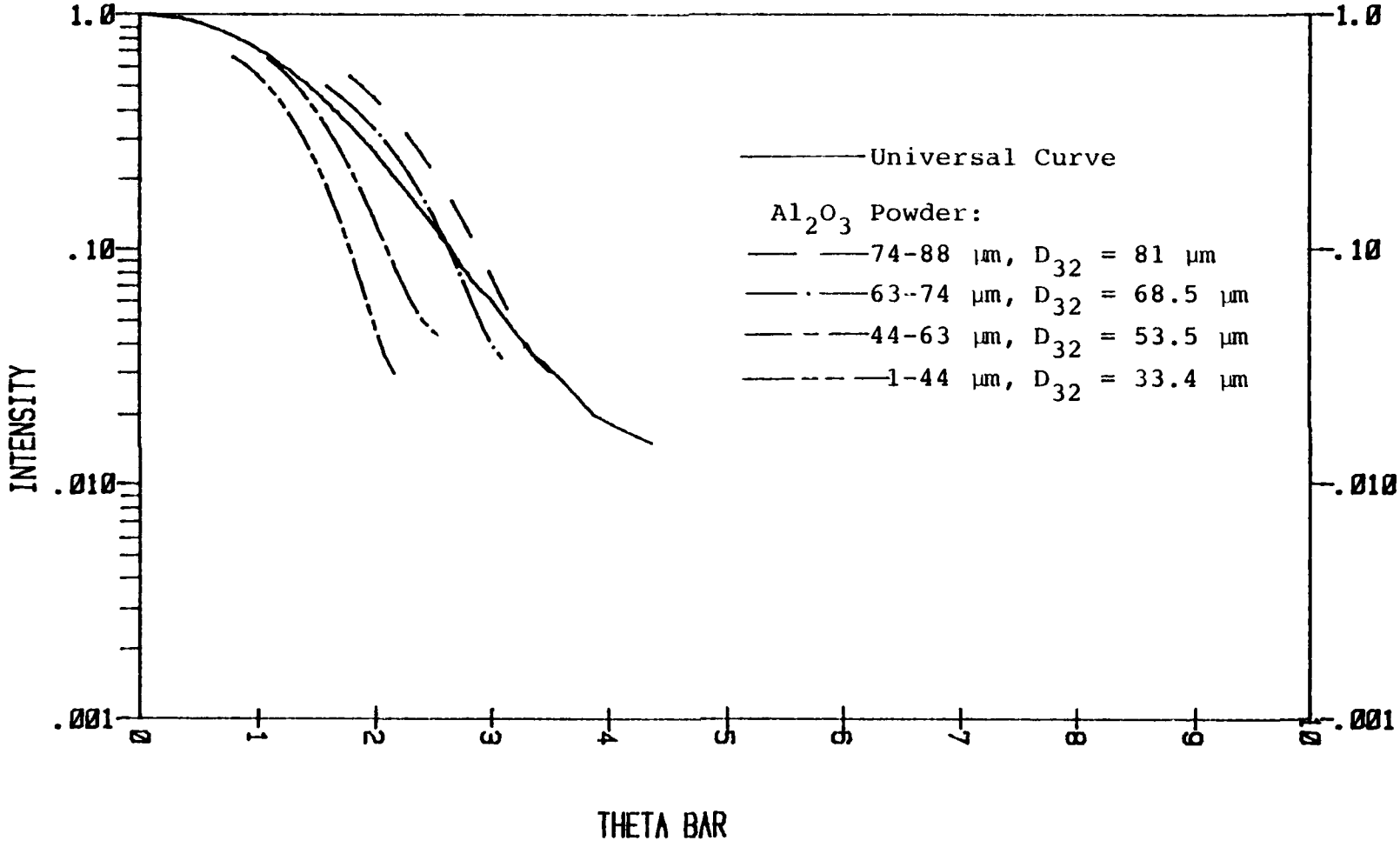

Figure 16: $I(\theta)$ vs $\bar{\theta}$, Al_2O_3 Powder

Figure 17: SEM Photograph--Clean Sample (Typical)

Figure 18: SEM Photograph--As Collected (Typical)

LIST OF REFERENCES

1. Cheung, H., and Cohen, N. S., On the Performance of Solid Propellants Containing Metal Additives, AIAA Paper 64-116, January 1964, American Institute of Aeronautics and Astronautics, New York, New York.

2. Netzer, D. W., Diloretto, V. D., and Dubrov, E., Particle Behavior in Solid Propellant Rockets, paper presented at JANNAF Combustion Meeting, 17th, Hampton, Virginia, 22-26 September 1980.

3. Kincaid, J. F., and Derr, R. L., Combustion Efficiency of Highly Aluminized Solid Propellants, paper presented at JANNAF Combustion Meeting, 18th, Pasadena, California, 19-23 October 1981.

4. Price, E. W., Combustion of Aluminum in Solid Propellant Flames, paper presented at Advisory Group for Aerospace Research and Development Meeting, 53rd, Oslo, Norway, 2-5 April 1979.

5. Caveny, L. H., and Gany, A., "Break-up of Al/Al_2O_3 Agglomerates in Accelerating Flowfields," AIAA Journal, v. 17, no. 12, pp. 1368-1371, December 1979.

6. Hermsen, R. W., Aluminum Oxide Particle Size for Solid Rocket Motor Performance Prediction, AIAA Paper 81-0035, American Institute of Aeronautics and Astronautics, New York, New York.

7. Air Force Rocket Propulsion Laboratory Technical Report 81-103, One Dimensional Reacting Three Phase Flow with Mass Transfer Between Phases, by S. C. Hunter, S. S. Cherry, C. H. Waldman, and J. R. Kliegel, p. 181, April 1982.

8. Stockham, J. D., and Fochtman, E. G., Particle Size Analysis, pp. 1-9, Ann Arbor Science, 1978.

9. Gumprecht, R. O., and Sliepcevich, C. M., "Scattering of Light by Large Spherical Particles," Journal of Physical Chemistry, v. 57, pp. 90-94, January 1953.

10. Gumprecht, R. O., and Sliepcevich, C. M., "Measurement of Particle Sizes in Polydispersed Systems by Means of Light Transmission Measurements Combined with Differential Settling," Journal of Physical Chemistry, v. 59, pp. 95-97, January 1953.

11. Chin, J. H., Sliepcevich, C. M., and Tribus, M., "Determination of Particle Size Distributions in Polydispersed Systems by Means of Measurements of Angular Variation of Forward Scattered Light at Very Small Angles," Journal of Physical Chemistry, v. 59, no. 9, pp. 845-848, September 1955.

12. Dobbins, R. A., Crocco, L., and Glassman, I., "Measurement of Mean Particle Sizes of Sprays from Diffractively Scattered Light," AIAA Journal, v. 1, no. 8, pp. 1882-1886, August 1963.

13. Roberts, J. H., and Webb, M. J., "Measurement of Droplet Size for Wide Range Particle Distributions," AIAA Journal, v. 2, no. 3, pp. 583-586, March 1964.

14. Mugele, R. A., and Evans, H. D., "Droplet Size Distribution in Sprays," Industrial and Engineering Chemistry, v. 43, pp. 1317-1324, 1951.

15. Dobbins, R. A., and Jizmagian, G. S., "Optical Scattering Cross Sections for Polydispersions of Dielectric Spheres," Journal of the Optical Society of America, v. 56, no. 10, pp. 1351-1354, October 1966.

17. Hodkinson, J. R., "Particle Sizing by Means of the Forward Scattering Lobe," Applied Optics, v. 5, no. 5, pp. 839-844, May 1966.

18. Air Force Office of Scientific Research Technical Report 79-0004, Mean Droplet Diameter Resulting from Atomization of a Transverse Liquid Jet in a Supersonic Air Stream, by A. S. Nejad, J. A. Schetz, and A. K. Jakubowski, November 1978.

19. Powell, E. A., Cassanova, R. A., Bankston, C. P., and Zinn, B. T., Combustion Generated Smoke Diagnostics by Means of Optical Measurement Techniques, paper presented at AIAA Aerospace Sciences Meeting, 14th, Washington, D.C., 26-28 January 1976.

20. Karagounis, S. G., An Investigation of Particulate Behavior in Solid Propellant Rocket Motors, Engineer Thesis, Naval Postgraduate School, Monterey, California, 1981.

21. Dobbins, R. A., "Measurement of Mean Particle Size in a Gas-Particle Flow," AIAA Journal, v. 1, no. 8, pp. 1940-1943, August 1963.

22. Cashdollar, K. L., Lee, C. K., and Singer, J. M., "Three-Wavelength Light Transmission Technique to Measure Smoke Particle Size and Concentration," Applied Optics, v. 18, no. 11, pp. 1763-1769, June 1979.

23. Plass, G. N., "Mie Scattering and Absorption Cross Sections for Aluminum Oxide and Magnesium Oxide," Applied Optics, v. 3, no. 7, pp. 867-871, July 1964.

24. Plass, G. N., "Temperature Dependence of the Mie Scattering and Absorption Cross Section of Aluminum Oxide," Applied Optics, v. 4, no. 12, pp. 1616-1619, December 1965.

25. Plass, G. N., "Mie Scattering and Absorption Cross Sections for Absorbing Particles," Applied Optics, v. 5, no. 2, pp. 279-285, February 1966.

26. Hansen, B. J., Automatic Control and Data Acquisition System for Combustion Laboratory Applications, Engineer Thesis, Naval Postgraduate School, Monterey, 1982.

INITIAL DISTRIBUTION LIST

		No. Copies
1.	Defense Technical Information Center Cameron Station Alexandria, Virginia 22314	2
2.	Library, Code 0142 Naval Postgraduate School Monterey, California 93940	2
3.	Department Chairman, Code 67 Department of Aeronautics Naval Postgraduate School Monterey, California 93940	1
4.	Professor D. W. Netzer, Code 67Nt Department of Aeronautics Naval Postgraduate School Monterey, California 93940	2
5.	CPT R. G. Cramer, Jr. 4903 Meadowbrook NW Lawton, Oklahoma 73505	8
6.	MAJ H. S. O'Neill 80 Rutgers Avenue Bridgeton, New Jersey 08302	1
7.	Deputy Under Secretary of the Army for Operations Research Room 2E261, Pentagon Washington, D.C. 20310	1

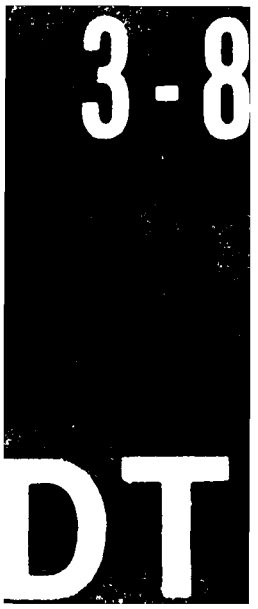
3-8
DT